Int. J. Electrochem. Sci., 7 **(2012)** 9290 - 9302

International Journal of ELECTROCHEMICAL SCIENCE
www.electrochemsci.org

Effects of Heat Treatment and Crystallographic Orientation on Creep Behavior of Aluminized Nickel-Base Single Crystal Superalloy CM186LC

Fahamsyah H. Latief[*], *Koji Kakehi*

Department of Mechanical Engineering, Tokyo Metropolitan University, 1-1 Minami-osawa, Hachioji-shi, Tokyo 192-0397, Japan
[*]E-mail: fahamsyah78@gmail.com

Received: 6 August 2012 / *Accepted:* 7 September 2012 / *Published:* 1 October 2012

The effect of heat treatment and crystallographic orientation on creep behavior of aluminized Ni-base single crystal superalloy CM186LC has been investigated in the present study. The aluminized superalloy has a better creep rupture life after HT2 rather than after HT1 which is indicated by the reduction of the γ′ cuboidal precipitates size. The coating treatment resulted in a significant decrease in creep rupture lives for all specimens. Generally, the specimens with (001) side-surface had a longer creep rupture life than the specimens with (011) side-surface, which means the results were anisotropic with respect to the secondary orientation which is normal to the primary orientation. The anisotropic creep behavior was affected by the microstructural change and the different arrangement of {111}<101> slip systems. First, the microstructural change after creep rupture test which is designated by the formation of TCP phase with a preferential orientation and SDZ. Second, the different arrangement of {111}<101> slip systems between the two side-surface specimens where the operation of {111}<101> slip system would be more activated in (011) side-surface specimen than that in (001) side-surface specimen.

Keywords: Ni-base superalloy, aluminide coating, creep properties, crystallographic orientation, microstructure, fracture surface

1. INTRODUCTION

Ni-base single crystal superalloys have been widely used for production of gas turbines, turbine blades and aero-engines due to their superior properties performance at high temperature. In general, single crystal superalloys exhibit better creep rupture, fatigue, and oxidation resistance over the conventional cast superalloys [1]. The turbine blades govern performances of turbine section of the jet engine and have profound impact on the thermal efficiency [2]. Thus, recent trends to further enhance

the engine efficiency by increasing the turbine inlet temperatures have placed greater demand for new superalloys with improved elevated temperature properties, particularly creep behavior [2]. Despite Ni-based superalloys have excellent mechanical strength at high temperatures but they tend to be vulnerable to environment attack due to the addition of refractory elements that provide their high temperature strength. The protective coatings are necessary to be applied on the surface of superalloys to protect against oxidation and hot corrosion in high temperature applications. Aluminide coatings have been extensively used in Ni-based superalloys for high temperature applications [3,4]. Aluminide coatings which prepared by pack cementation process [5] are used to generate good protection against high temperature oxidation and hot corrosion because of the practical commercial benefits rather than other coating processes.

Thereunto, the level of the grain boundary strengthening elements such as B, Hf and Zr tend to increase of solidus temperature, have been reduced since the absence of grain boundaries in single crystal superalloys [6]. The high melting temperature of single crystal superalloys frequently enables for refinement of the γ' microstructure within the γ matrix with a solution anneal heat treatment and subsequent one or more aging heat treatments. The heat treatments in Ni-base single superalloys are principally suggested to produce high volume fraction and better size distribution of γ' precipitates which optimize the mechanical properties. A solution heat treatment is intended to dissolve the precipitating phase for subsequent re-precipitation in an optimized morphology and size. Besides, the solution heat treatment also results in elimination or reduction of the segregation to obtain a more homogeneous microstructure [7]. Previous work has reported that the heat treatment has a significant impact on the morphology, volume fraction, size and distribution of the strengthening phase [8]. Therefore, an appropriate heat treatment schedule is able to improve the mechanical properties of single crystal superalloys at room and elevated temperature [6].

Although several attempts have been made to investigate the influence of heat treatment on the microstructure and mechanical properties of single crystal Ni-base superalloys [3,7,9], but the study of heat treatment effect on the mechanical properties of aluminized Ni-base single crystal superalloys with different surface orientations has hitherto been relatively scarce. Therefore, the main objective of this study is to investigate the effect of heat treatment and crystallographic orientation on creep behavior of aluminized Ni-base single crystal superalloy.

2. EXPERIMENTAL DETAILS

2.1. Material

A Ni-base single crystal superalloy CM186LC was used as an experimental material. The chemical composition of superalloy in mass % is 5.74 Al, 0.73 Ti, 6 Cr, 9.3 Co, 1.4 Hf, 3.4 Ta, 2.9 Re, 8.3 W, 0.005 Zr, 0.016 B, 0.019 Fe, 0.07 C and balance Ni. The Ni-base single crystal superalloy CM186LC was produced in a cylindrical rod which is directionally solidified in [001]-direction with a diameter of 21 mm and a length of 80 mm.

2.2. Heat treatment schedule

Two kinds of heat treatment procedures were carried out in this study. Later, the first and second procedures of heat treatment were named as HT1 and HT2, respectively. The details of heat treatment procedures were given in Table 1.

Table 1. Heat treatment procedures of Ni-base single crystal superalloy CM186LC

Route	Heat treatment procedure
HT1	Aging treatment at 1080 °C/4 h AC + 871 °C/20 h AC
HT2	Solution treatment at 1274 °C/8 h AC and followed by aging treatment at 1080 °C/4 h AC + 871 °C/20 h AC

2.3. Sample preparation

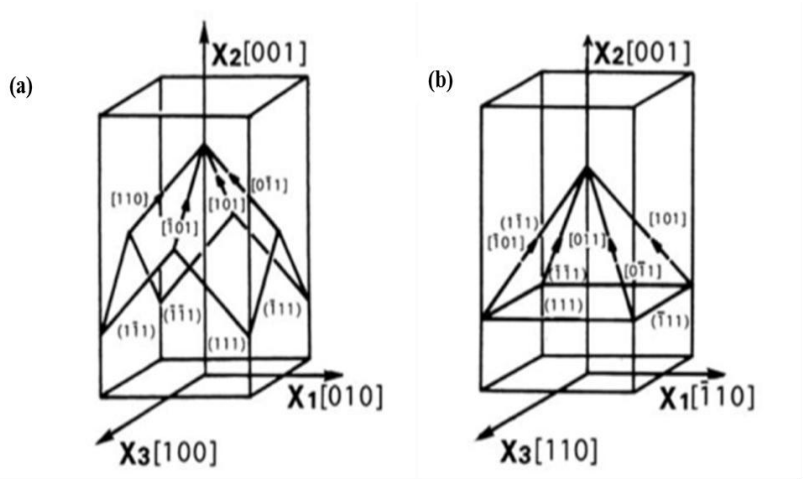

Figure 1. Arrangement of {111}<101> slip systems for two kinds of specimens: (a) (001) and (b) (011) side-surface creep specimens.

The crystallographic orientation of superalloys was analyzed by the X-ray Laue reflection method. The creep specimens with (001) and (011) side-surface orientations (Fig. 1) were then cut from the rod by electric discharge machining (EDM) with a cross section area of 2.8 mm x 2.8 mm and the gauge length of 19.6 mm. The creep specimens were mechanically polished down to 1200 mesh by emery paper and ultrasonically cleaned in acetone bath for 10 min prior to aluminizing treatment.

2.4. Aluminizing treatment

The polished specimens were embedded in a Al_2O_3 retort containing a mixture of 24.5 wt.% Al, 24.5 wt.% Fe, 49 wt.% Al_2O_3 and 2 wt.% NH_4Cl powders and heated at 1000°C for 5 h in flowing argon during aluminizing treatment. This aluminizing treatment is also known as pack cementation.

2.5. Creep rupture test

In this study, the creep rupture test was conducted at an intermediate temperature of 900 °C and a stress of 320 MPa with a parallel load direction to <001> direction. The aluminized specimens were tested under constant load in air. The bare specimens were also examined in order to compare the creep behavior with the aluminized ones.

2.6. Hardness measurement

The hardness value was measured by a micro-indenter machine under an applied load of 100 gf and a dwell time of 15 s. Hardness measurements were applied on the coating-substrate to evaluate the gradient of the hardness in order to confirm the creep behavior on different surface orientations.

2.7. Microstructure observation

The microstructures of parent material, aluminized specimens and ruptured aluminized specimens were observed by optical microscopy (OM) and scanning electron microscopy (SEM).

3. RESULTS

3.1. Microstructures after heat treatment

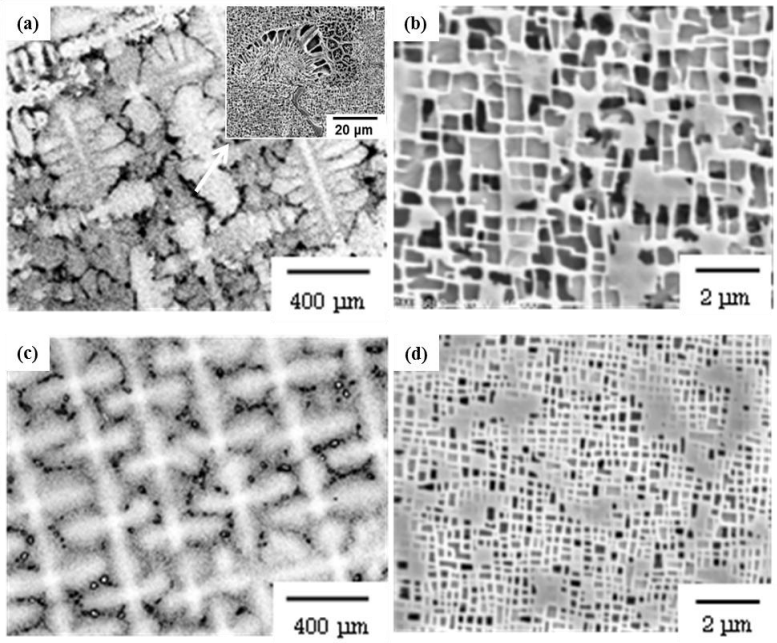

Figure 2. Optical and SEM micrographs of Ni-base single crystal superalloy CM186LC: (a,b) after HT1 and (c,d) after HT2, respectively.

The optical and SEM micrographs of Ni-base single crystal superalloy CM186LC after different heat treatment routes were shown in Figure 2. A two-phase γ/γ′ microstructure with a dendritic segregation pattern and a limited amount of γ/γ′ eutectic solidification spreading out in some interdendritic regions were obviously seen in the specimens of HT1 (Fig. 2a) and HT2 (Fig. 2c). In general, the microstructure of single-crystal superalloy CM186LC consists of about 70% volume fraction of strengthening γ′ cuboidal precipitates within a γ matrix. The dark area was appeared between dendritic and interdendritic regions called as γ′+γ eutectic precipitates in the γ matrix. The enlarged eutectic region (as indicated by white arrow) was inserted in Fig. 1a. The γ′ cuboidal precipitates embedded coherently in γ matrix and aligned along <001> direction during the aging treatment due to the elastic interaction between precipitates. Furthermore, the contrast between γ phase and γ′ phase was tangible. The γ′ cuboidal precipitates of HT1 specimens (Fig. 2b) were larger than that of HT2 specimen (Fig. 2d). It attested that the solution heat treatment was effective to refine the size of γ′ cuboidal precipitates within the γ matrix.

3.2. Microstructures after aluminizing treatment

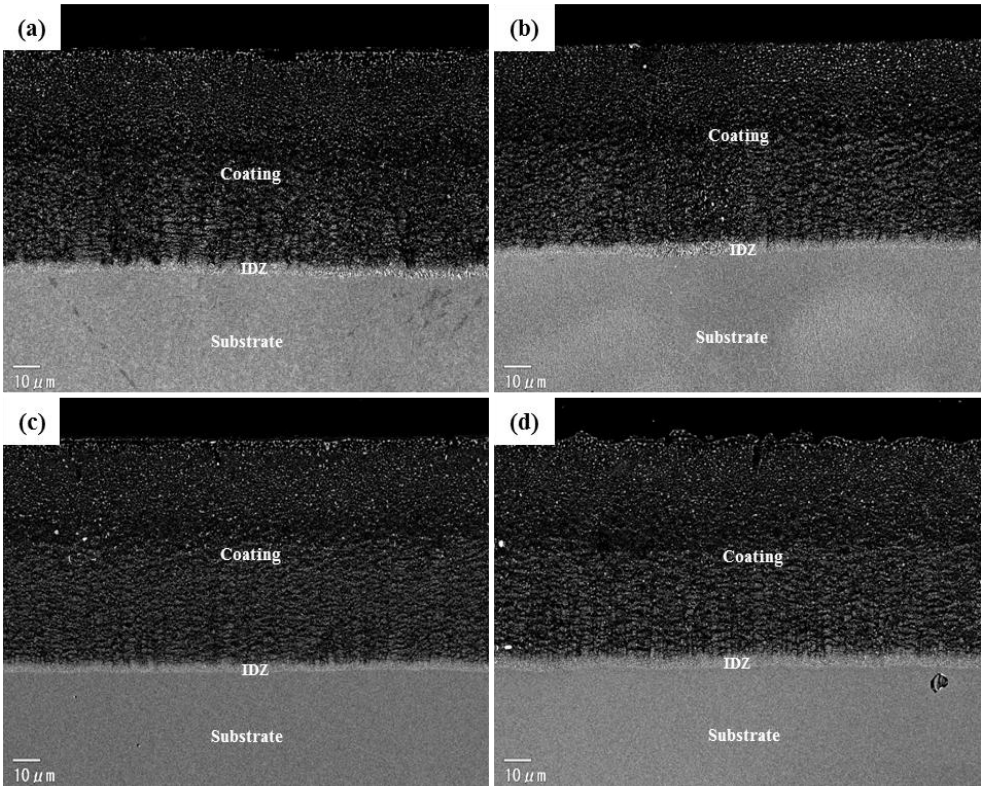

Figure 3. SEM micrographs of aluminized Ni-base single crystal superalloy CM186LC: (a,b) HT1 specimens and (c,d) HT2 specimens with (a,c) (001) side-surface and (b,d) (011) side-surface.

The SEM cross-section micrographs of aluminized superalloy after aluminizing treatment were presented in Figure 3. There was a new zone formed between coating and substrate, termed as interdiffusion zone (IDZ). The IDZ is defined as that layer between the coating and the substrate not

initially aluminized, but which transforms to β (NiAl) during subsequent heat treatment. The thickness of IDZ was varied with the different of heat treatment procedures in (001) and (011) side-surfaces as shown in Figure 3. The IDZ thickness of HT1 specimens was about 4±0.4 μm for (001) side-surface and 5±0.3 μm for (011) side-surface, whereas the IDZ thickness of HT2 specimens was about 3±0.2 μm for (001) side-surface and 5.5±0.15 μm for (011) side-surface.

3.3. Creep behavior

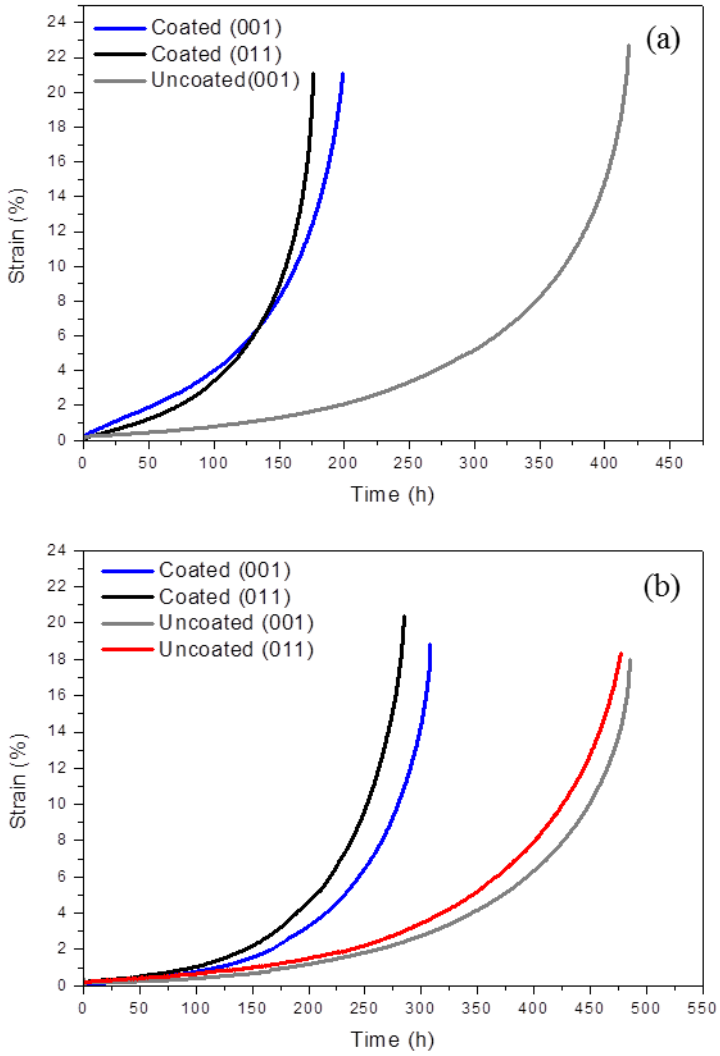

Figure 4. Creep rupture curves of Ni-base single crystal superalloy CM186LC: (a) after HT1 and (b) after HT2.

The creep rupture lives of Ni-base single crystal superalloy CM186LC with different heat treatment procedures at an intermediate temperature of 900°C and a stress of 320 MPa are shown in Figure 4. In general, the aluminized specimens with both heat treatment procedures showed lower creep rupture life than those of the bare specimens. It indicated that the aluminizing treatment has a deleterious effect to the creep behavior of Ni-base single crystal superalloy CM186LC. Meanwhile, the

aluminized specimens with (001) side-surface exhibited slightly longer creep rupture lives than the bare specimens with (011) side-surface at both heat treatment procedures. Although the difference in creep rupture life was not large enough between (001) and (011) side-surfaces but it verified that the crystallographic orientation affected the mechanical properties of the superalloys. In the other words, the anisotropic creep behavior was occurred and distinctly demonstrated by the difference in creep rupture life at different surface orientations in aluminized Ni-base single crystal superalloy CM186LC. Furthermore, the HT2 specimens have better creep rupture life compared to the HT1 specimens. In short, the HT2 treatment was able to improve the creep rupture life of the Ni-base single crystal superalloy CM186LC both in aluminized and bare specimens because of the refinement of the size of γ′ cuboidal precipitates within the γ matrix.

3.4. Microstructures after creep ruptures test

The SEM micrographs of aluminized Ni-base single crystal superalloy CM186LC after creep rupture test with different heat treatment procedures are shown in Figure 5.

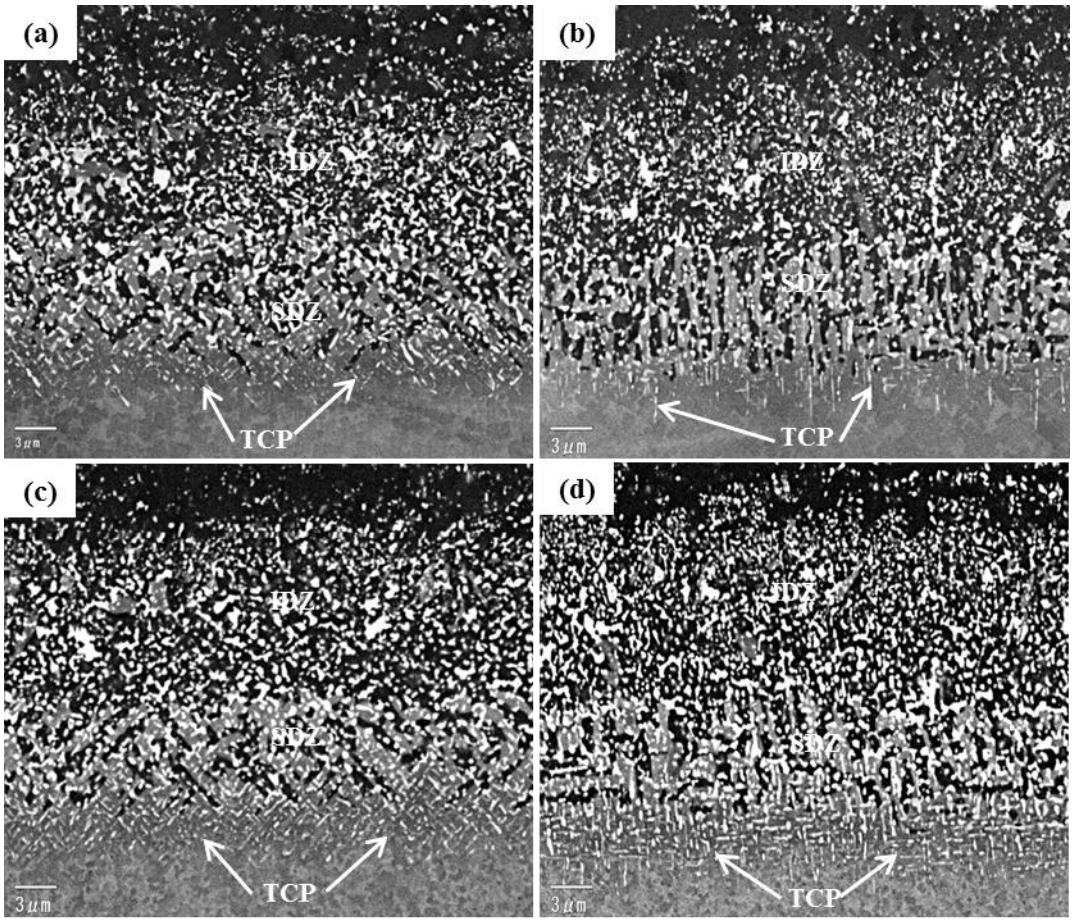

Figure 5. SEM micrographs of ruptured aluminized Ni-base single crystal superalloy CM186LC: (a,b) HT1 specimens and (c,d) HT2 specimens with (a,c) (001) side-surface and (b,d) (011) side-surface.

The extension of diffusion zone was occurred for all specimens where the substrate diffusion zone (SDZ) was formed after creep rupture test. The SDZ is a layer that lies beneath the IDZ where the matrix has not transformed to β but nevertheless has a raised level of aluminum. SDZ should be differentiated from IDZ because it is of significance that it remains particularly γ′ and retains the orientation of the single crystal substrate. The diffusion layer thickness for HT1 specimens was about 16±1.2 μm for (001) side-surface and 17±0.85 μm for (011) side-surface whereas for HT2 specimens was about 15±1.4 μm for (001) side-surface and 16±1.1 μm for (011) side-surface. The TCP phases were also found in all specimens after creep rupture test with a particular arrangement of TCP phase between the two surface orientations as seen in Figure 5. Most importantly, the secondary reaction zone (SRZ) was not observed both in (001) and (011) side-surfaces.

3.5. Fracture surfaces

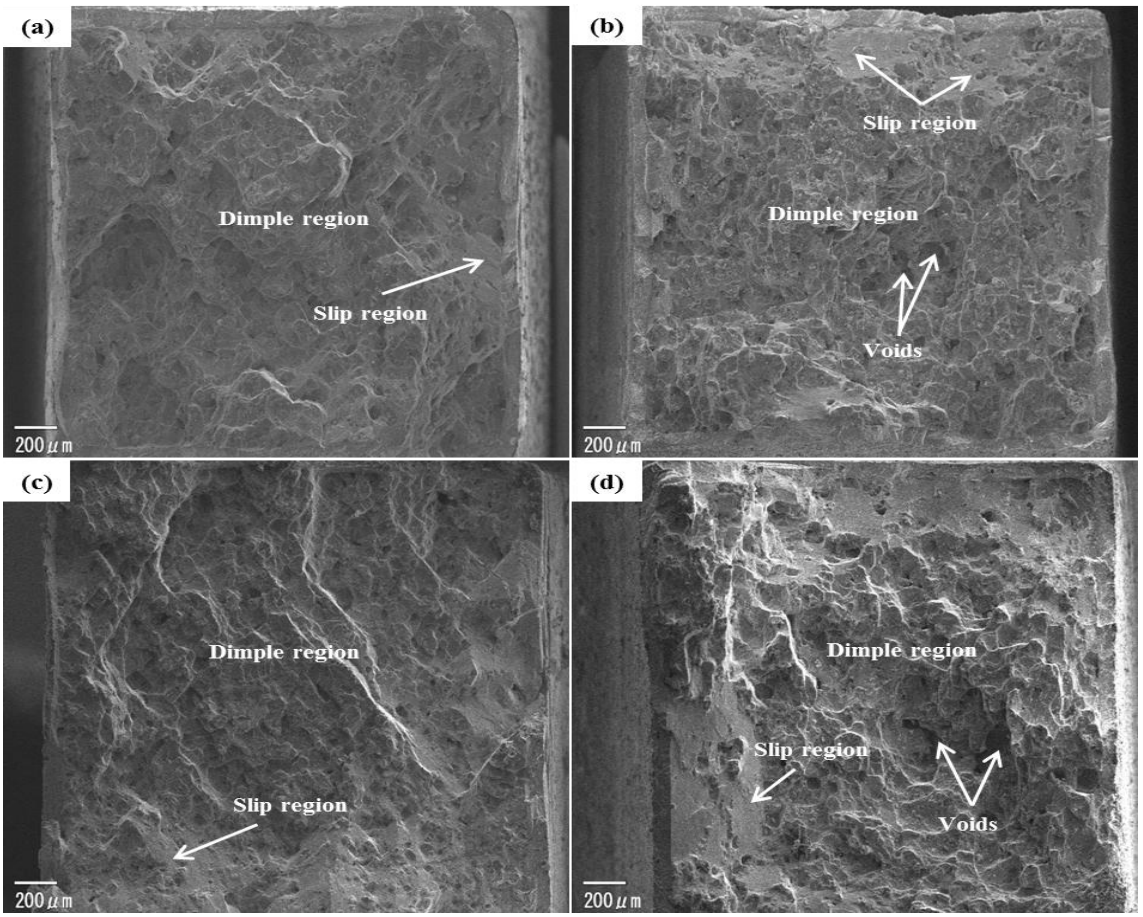

Figure 6. Fracture surfaces of ruptured aluminized Ni-base single crystal superalloy CM186LC: (a,b) HT1 specimens and (c,d) HT2 specimens with (a,c) (001) side-surface and (b,d) (011) side-surface.

Figure 6 shows the fracture surfaces of two surface orientations ruptured aluminized specimens at 900°C/320 MPa with different heat treatment procedures. The fracture surfaces exhibited two different fracture modes which can be categorized as dimple fracture region (mode 1) and slip region

(mode 2). The presence of the two different fracture modes on the fracture surface concurrently proposes a mixed mode of failure operating during creep rupture tests at 900°C.

3.6. Vickers hardness

Vickers hardness measurements were employed on the longitudinal sections in the coating-substrate regions. The results revealed that the diffusion layer in aluminized specimens has a higher hardness value compared to the coating and the substrate as shown in Table 2. Moreover, the hardness of interdiffusion zone (IDZ) was the highest among the other regions.

Table 2. Vickers hardness of the coating-substrate region of CM186LC superalloy

Specimen and surface orientation	Vickers hardness of coating-substrate regions (HV)			
	Coating	IDZ	SDZ	Substrate
As-aluminized HT1-(001)	442.4	850.3	-	431.9
As-aluminized HT1-(011)	433.8	837.5	-	425.4
As-aluminized HT2-(001)	467.3	891.2	-	461.8
As-aluminized HT2-(011)	454.1	860	-	450.6
Ruptured HT1-(001)	414.6	698.4	643.2	405.1
Ruptured HT1-(011)	402.8	683.6	631.9	392.7
Ruptured HT2-(001)	430.2	718.7	627.5	418.3
Ruptured HT2-(011)	418.5	700.9	610.1	405.2

4. DISCUSSION

4.1. Effect of aluminizing treatment

The function of the protective coating is to act as a buffer between the substrate and the surroundings to prevent degradation in a harsh environment. Despite the protective coating is not particularly designed to improve the mechanical properties of the material, its strain behavior and toughness are important with respect to its ability to protect the surface and to prevent crack initiation under mechanical loading [10]. As shown in Figure 4, the creep rupture lives of the aluminized specimens are lower than those of the bare specimens for both heat treatment procedures. The decrease of creep rupture lives in aluminized specimens might be induced by the diffusion of aluminum from the protective coating into the substrate which might be due to weakening of atomic bonds, since the aluminum is a metal with low melting point so its effect could be considered as similar to that of other low melting metals [11]. Thus, the increment of the aluminum concentration in the interdiffusion zone (IDZ) could lead to reduction in strength and premature failure of the specimen.

As reported by Kang [10], for the coated condition, crack nucleation occurred in the coating layer rather than in the parent substrate for the conventionally and directionally solidified nickel-base alloys, Rene 80. The main reason for the preferential formation of microcracks in the coated layer is associated with the higher hardness of the diffusion zone in the coating layer relative to the substrate

[10] as shown in Table 2. When the aluminized specimens are applied to high temperature environments and stress [12], the interdiffusion of elements between the single crystal substrate and the coating layer took place. However, the outward diffusion of Ni from the substrate leads to the enrichment of refractory elements and promotes the formation of topologically close-packed (TCP) phases. Some reports have confirmed that the elements Re and W may promote the precipitation of TCP phase [12]. The creep strength of superalloys diminished when the TCP phases are precipitated [13,14].

4.2. Effect of heat treatment

The morphology, size and distribution of γ' phase have greatly changed after solution heat treatment. The solution heat treatment is aimed to both dissolve the γ' formed during cooling from solidification and the eutectic γ/γ', as well as to reduce the degree of chemical segregation due to the partitioning of some of the elements to the dendrite core and interdendritic regions [6]. Moreover, the creep properties of superalloy depend on the morphology, size, distribution and fraction volume of γ' strengthening phase [8]. The creep rupture lives of the HT1 aluminized specimens were 199 h for (001) side-surface and 175 h for (011) side-surface whereas the HT2 aluminized specimens was 310 h for (001) side-surface and 284 h for (011) side-surface. However, the size of γ′ cuboidal precipitates was about 0.5 – 1 μm after HT1 and 200 – 400 nm after HT2. It was clear that the size of γ' phase has a significant effect on the creep rupture life of aluminized Ni-base single crystal superalloy. Therefore, the creep strength of aluminized Ni-base single crystal superalloy CM186LC improved after HT2 treatment.

4.3. Effect of crystallographic orientation

Some papers have declared that the mechanical properties of Ni-base single crystal superalloys are distinctly influenced by crystallographic orientation [15,16]. The creep strength results show that the {001} specimens has slightly longer creep rupture lives than those {011} specimens. It should be noted that the creep testing temperature has important role to the crystallographic orientation effect. It has also been reported that the creep strength of tested samples is highly anisotropic at lower temperature, while at high temperature, the anisotropic creep behavior is significantly decreased, and the misorientation dependence of creep deformation is also less pronounced. The main reason of this occurrence is due to the increase of the activity slip systems at high temperatures [17]. It can be obviously seen from the difference in creep rupture life both in HT1 and HT2 conditions since the creep rupture tests were performed at an intermediate temperature of 900 °C.

To clarify the anisotropic creep properties, there are two possible reasons should be considered that is the microstructural changes after creep rupture test and the deformation fracture mechanism. First, the microstructural changes which are related to the formation of TCP phases and SDZ. The σ phase, one of the TCP phases, forms coherently on {111} planes in platinum-modified aluminized Ni-based single-crystal substrates [18]. The schematic illustration of TCP phase growth in both side-

surfaces is presented in Figure 7. The TCP phases grow up with a cross mark arrangement in (001) side-surface and having a perpendicular configuration as well as parallel to the substrate in (011) side-surface. The TCP preferred precipitation orientation induced the extension of diffusion zone with the formation of SDZ beneath IDZ which occurred during plastic deformation. Indeed, the presence of SDZ results in the degradation of creep rupture life of the aluminized superalloys. This phenomenon is caused by the difference in SDZ thickness which influenced by the geometry of TCP phase within SDZ. Further observation exhibited that the TCP phase in (011) side-surface has a deeper penetration depth than that in (001) side-surface as shown in Figure 5. Therefore, the depth of TCP phase penetration might have a significant role of high diffusion path for refractory elements to enhance further growth of diffusion layers in (011) side-surface orientation. The interface between TCP phase and the matrix at high temperatures is regularly associated with interfacial decohesion which may potentially act as initiation sites for crack [19].

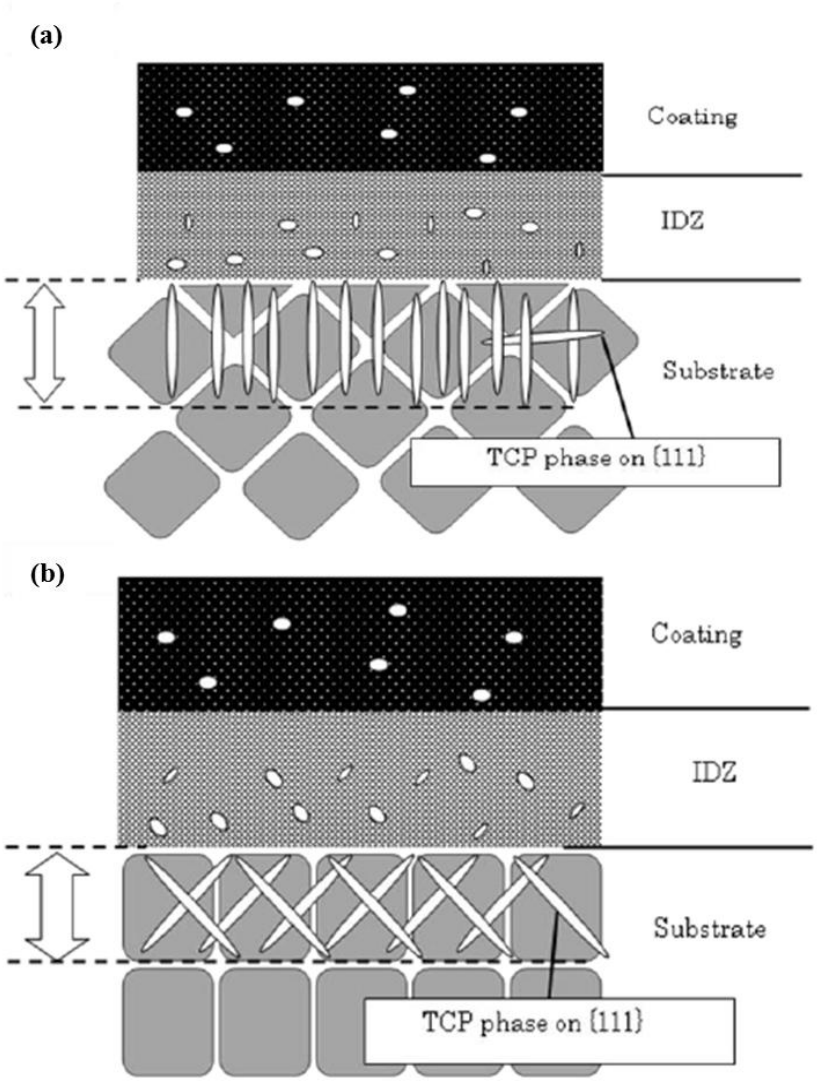

Figure 7. Schematic illustration of TCP preferred precipitation orientation: (a) (001) side-surface and (b) (011) side-surface.

Second, the deformation fracture mechanism has a close relationship with the slip systems arrangement (Fig. 1) and it can be seriously considered as one of reasons in order to elucidate the anisotropic creep properties. As shown in Figure 6, the fracture surfaces exhibited two different fracture modes. In the mode 1, the micro-voids are formed and coalesced in the interior of the substrate. Whereas in the mode 2, the crack propagates along {111} crystallographic planes which is the normal direction makes an angle of 54.7° with the tensile stress axis. Thus, the operation of {111}<101> slip system would result in the slip-band decohesion fracture along {111} slip planes near the surface. The ratio of crystallographic {111} facets associated with the activated slip system for HT1 specimens was about 5 % for (001) side-surface and 7 % for (110) side-surface. Meanwhile, the ratio of {111} facets associated with the activated slip system for HT2 specimens was about 14% for (001) side-surface and 16% for (011) side-surface. These ratios reveal that the specimens with (011) side-surface have a larger ratio of crystallographic {111} facets than that of the specimens with (001) side-surface. It indicates that the operation of {111}<101> slip system would be more activated in (011) side-surface specimen than that in (001) side-surface specimen.

5. CONCLUSIONS

The following conclusion can be withdrawn from this study:

1. The microstructure of Ni-base single crystal superalloy CM186LC was improved after HT2 which is denoted by the decrease of cuboidal γ' phase size to be about 200 – 400 nm and distributed homogenously. This microstructure improvement has a great impact on the creep properties of the superalloy.
2. In general, the creep strength diminished by aluminizing treatment. In addition, the surface micro-crack induced by the higher-hardness layer in IDZ and TCP phase formation in SDZ decreased the creep rupture life in aluminized specimens.
3. The aluminized specimens with (001) side-surface exhibited longer creep rupture life than that with (011) side-surface, this phenomenon is due to the microstructural change after creep rupture test and the difference arrangement in the crystallographic geometry of {111} slip planes on which micro-cracks formed.

ACKNOWLEDGEMENT
The authors are grateful to Dr. Hideyuki Murakami, Hybrid Materials Center, National Institute for Materials Science (NIMS), Tsubuka, Japan, for assisting us in the aluminizing treatment.

References

1. E. W. Ross and K. S. O'Hara, *Superalloys 1996*, ed. by R. D. Kissinger, D. J. Bye, D. L. Anton, A. D. Cetel, M. V. Nathal, T. M. Pollock and D. A. Woodford, (TMS, Warrendale, PA, 1996) pp. 19-26.
2. R. C. Reed, The Superalloys, *Cambridge University Press*, 2006.

3. J. Angenete and K. Stiller, *Mater. Sci. Eng. A*, 316 (2001) 182-194.
4. D. K. Das, V. Singh, S. V. Joshi, *Metall. Mater. Trans.*, 29A (1998) 2173-2188.
5. H. Murakami and T. Sakai, *Scr. Mater.*, 59 (2008) 428-431.
6. G. E. Fuchs, *Mater. Sci. Eng. A*, 300 (2001) 52-60.
7. G. E. Fuchs, *J. Mater. Eng. Perform.*, 11 (2002) 19-25.
8. L. Z. He, Q. Zheng, X. F. Sun, H. R. Guan, Z. Q. Hu, A. K. Tieu, et al., *Mater. Sci. Eng. A*, 398 (2005) 128-136.
9. M. Doi, T. Miyazaki, T. Eakatsuki, *Mater. Sci. Eng.*, 67 (1984) 247–253.
10. S. B. Kang and Y. G. Kim, *Mater. Sci. Eng.*, 83 (1986) 75-86.
11. V. I. Nikitin and T. N. Grigor'eva, *Mater. Sci.*, 10 (1975) 5-9.
12. R. M. Kearsey, J. C. Beddoes, K. M. Jaansalu, et. al., *Proceedings of the Tenth International Symposium on Superalloys, Superalloys 2004*, ed. By T. M. Pollock, H. Harada, R. C. Reed and S. Walston, (Metals and Materials Society, United States; 2004) pp. 801–810.
13. M. Simonetti, P. Caron, *Mater. Sci. Eng. A*, 254 (1998) 1–12.
14. K. Zhao, Y. H. Ma, L. H. Lou, Z. Q. Hu, *Mater. Trans.*, 46 (2005) 54–58.
15. T. Hino, T. Kobayashi, Y. Koizumi, H. Harada and T. Yamagata, *Superalloys 2000*, ed. by K. A. Green, T. M. Pollock and R. D. Kissinger, (The Minerals, Metals, Materials Society, Warrendale, Pittsburg, 2000) pp. 729–736.
16. S. Wollmer, T. Mack, U. Glatzel, *Mater. Sci. Eng. A*, 319-321 (2001) 792–795.
17. V. Sass, U. Glatzel and M. Feller Kniepmeier, *Acta Mater.*, 44 (1996) 1967-1977.
18. C.M.F. Rae, M.S. Hook, R.C. Reed, *Mater. Sci. Eng. A*, 396 (2005) 231-239.
19. L. Mueller, T. Link, M. Feller-Kniepmeier, *Script. Metall. Mater.*, 26 (1992) 1297-1302.